Composites Part B 140 (2018) 214–222

Contents lists available at ScienceDirect

Composites Part B

journal homepage: www.elsevier.com/locate/compositesb

UV-curable photosensitive silicone resins based on a novel polymerizable photoinitiator and GO-modified TiO_2 nanoparticles

Tong Zhang, Bo Jiang*, Yudong Huang

MIIT Key Laboratory of Critical Materials Technology for New Energy Conversion and Storage, School of Chemistry and Chemical Engineering, Harbin Institute of Technology, Harbin 150001, PR China

ARTICLE INFO

Keywords:
Methacrylic-silicone resin
Polymerizable photoinitiator
UV-curing
Thermal stability

ABSTRACT

A novel polymerizable benzophenone photoinitiator containing acryloxy (BPA) was synthesized. The photopolymerization of photosensitive methacrylic-silicone resins (MASR) initiated by BPA was studied. Results show that BPA is an efficient photoinitiator, which could generate radicals from the photolysis reaction and be consumed via copolymerizing with MASR. The designed UV-curing silicone resins system initiated by BPA showed a high carbon-carbon double bonds conversion above 80% after 20 s UV radiation. In addition, reduced graphene oxide (rGO)-TiO_2 composites were elaborated by hydrothermal reaction. The synergistic effects from graphene and TiO_2 further enhanced the carbon-carbon double bonds conversion of MASR to 86% with 15 s UV irradiation, demonstrating that the incorporated rGO-TiO_2 significantly improve the formulation UV-curing reactivity. Additionally, UV-cured MASR with rGO-TiO_2 showed an excellent thermal stability. This work proposes an efficient strategy to improve the polymerization degree of UV-curable photosensitive silicone resins.

1. Introduction

Silicone resins, as an interesting class of non-carbonic polymers, provide remarkable properties including excellent dielectric properties, good thermal stability, impressive antiweatherability and chemical resistance [1–3]. The crosslinking chemistries of silicone-based materials can be categorized into three main chemical reactions: (1) hydrosilylation between vinyls and hydride-terminated siloxanes in the presence of the metal catalyst such as platinum [4], (2) thiol-ene click chemistry between vinyl group and thiol group [5], (3) condensation reaction of alkoxysilane [6]. However, these crosslinking chemistries still present pitfalls that prevent their use for specific applications and have many drawbacks such as the harmful of heavy metal catalysts to the environment, high curing temperature and high energy consumption. Therefore, most researches focus on UV-curable silicone resins and most UV-curable system involves reactive acrylate, methacrylate, or allyl groups [7,8].

The light induced polymerization technique have been considered as ecofriendly due to its outstanding features such as high efficiency, low energy consumption, solvent-free formulation, and room temperature treatment [9]. These characteristics promote photopolymerization over thermally induced processes which require much time and high temperature to complete the reaction. Significantly, photopolymerization materials have wide application in elaboration of coatings, adhesives, and other products [10–12].

As a crucial component of a UV-curable system, photoinitiators could absorb light and generate active radicals to initiate the polymerization [13]. However, low-molecular-weight photoinitiators are generally treated as a problem in photopolymerization due to the disadvantages such as odor, yellowing, poor compatibility with the UV-curable resin and migration in the post-cured process [14]. Thus, polymerizable photoinitiators have been developed as a valuable alternative to overcome the disadvantages, which can not only generate free radicals to initiate photopolymerization, but also copolymerize with the polymer [15].

TiO_2 has also been testified to be free-radical photoinitiators for curing (meth)acrylic resins, due to its ability of generating electron-hole pairs under photoexcitation, which could react with resin monomers providing reactive radicals [7]. Due to the unique synergistic effect, incorporation of the graphene and TiO_2 is considered a promising nanocomposite [16]. Graphene, which is often prepared by reducing graphene oxide, have drawn interest from researchers owing to its large specific surface area, excellent electrical conductivity, high charge carriers mobility and high mechanical strength [17–19]. It turns out to be an electron acceptor/transporter for TiO_2 particles and anticipates to significantly enhancing the lifetime of electron-hole pairs [20]. Thus, it is a potential candidate to facilitate the adsorption capability and enhance the photoactivity of TiO_2 under UV light due to the unique

* Corresponding author.
E-mail address: jiangbo5981@hit.edu.cn (B. Jiang).

https://doi.org/10.1016/j.compositesb.2017.12.006
Received 13 June 2017; Received in revised form 30 October 2017; Accepted 15 December 2017
Available online 20 December 2017
1359-8368/

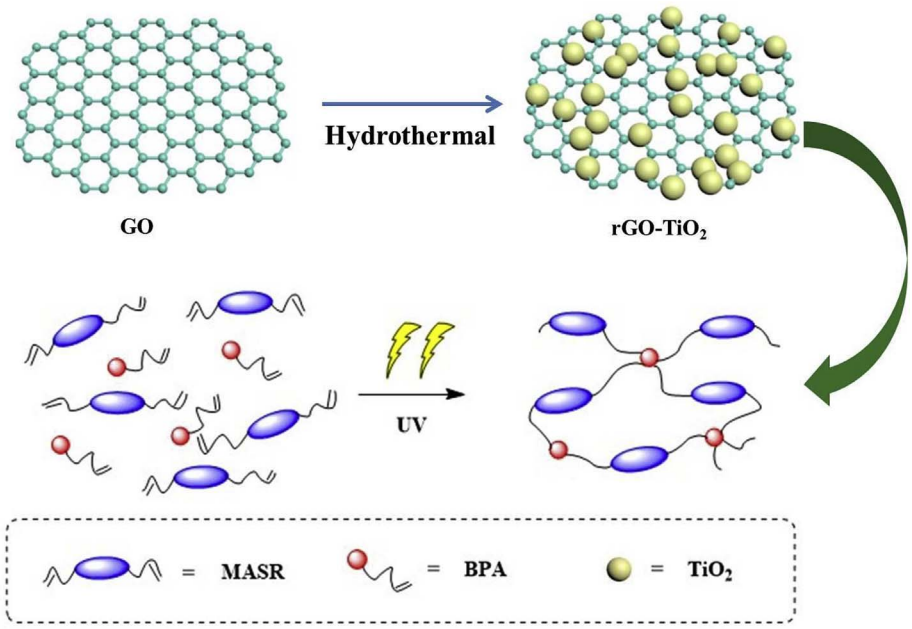

Fig. 1. Schematic of the preparation procedure of UV-cured MASR.

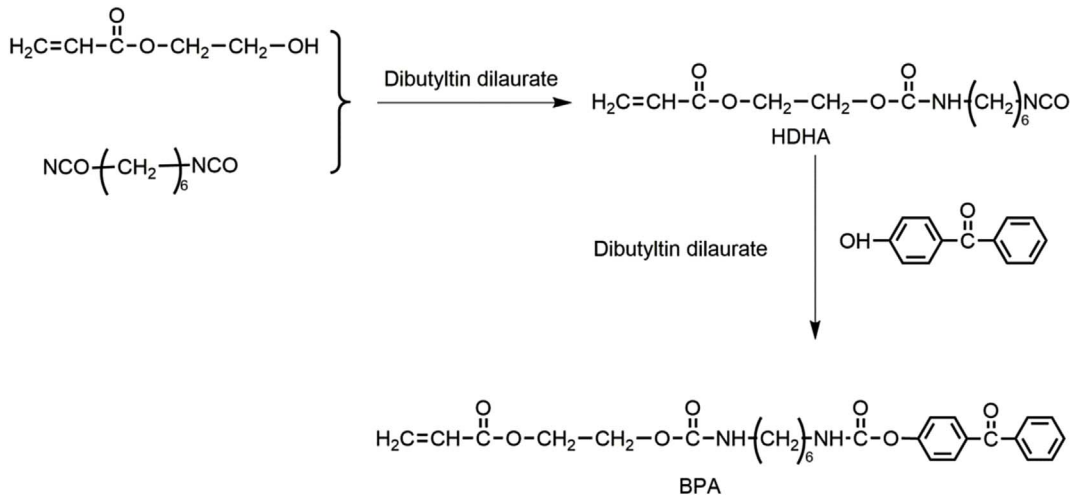

Fig. 2. The synthesis routes of BPA.

electron-transferring property. In addition, the incorporation of graphene could avoid TiO_2 particles suffering aggregation in an organic matrix, which consequently leads to good dispersity.

In this study, polymerizable photoinitiator was synthesized to initiate the polymerization of UV-curable photosensitive methacrylic-silicone resins. The effects of BPA and rGO-TiO_2 composites on the photopolymerization of MASR were investigated. The photoinitiation mechanism and the photopolymerization behavior were also presented. The schematic representation of UV-cured methacrylic-silicone resins based on a BPA and rGO-TiO_2 was shown in Fig. 1.

2. Experimental

2.1. Materials

Methyltriethoxysilane (MTES), dimethyldiethoxylsilane (DDS), 3-methacryloxypropyltrimethoxysilane (MPTS) were obtained from Qufu Chenguang Chemical Co., Ltd. (China). Hexamethylene diisocyanate (HDI), 4-hydroxybenzophenone, 2-hydroxyethyl acrylate (2-HEA), dibutyltin dilaurate, dibutylamine and 2-(dimethylamino)ethyl methacrylate (DMAEMA) were supplied by Aladdin Reagent Shanghai Co., Ltd (China). Tetrabutyl titanate ($Ti(OC_4H_9)_4$), potassium permanganate, and concentrated sulfuric acid (98 wt%) were obtained from Sinopharm Chemical Reagent Co., Ltd (China). All chemical reagents were used as received.

2.2. UV-Curing of MASR based on BPA and GO- TiO_2

MASR with initiator (0.5 μm film on glass) was irradiated by a light source of high-pressure mercury lamp (1000 W) with a distance of 10 cm from lamp to specimen at room temperature in air atmosphere. The composition of the samples investigated in the work was shown in Table S2. DMAEMA as the coinitiator, [BPA]/[DMAEMA] = 1:4 mol/mol [21].

2.2.1. Preparation of MASR

MTES, DDS and MPTS with different mole ratio 7:2:1 and 6:3:1 (supported in Table S1) were added into a flask connecting to mechanical stirrer and refluxing condenser. Then hydrochloric acid solution (10 wt%, diluted by ultrapure water) was slowly added dropwise through the constant-pressure funnel to adjust the pH value to 3–4. The blend was then refluxed at 60 °C for 4 h. The transparent viscous

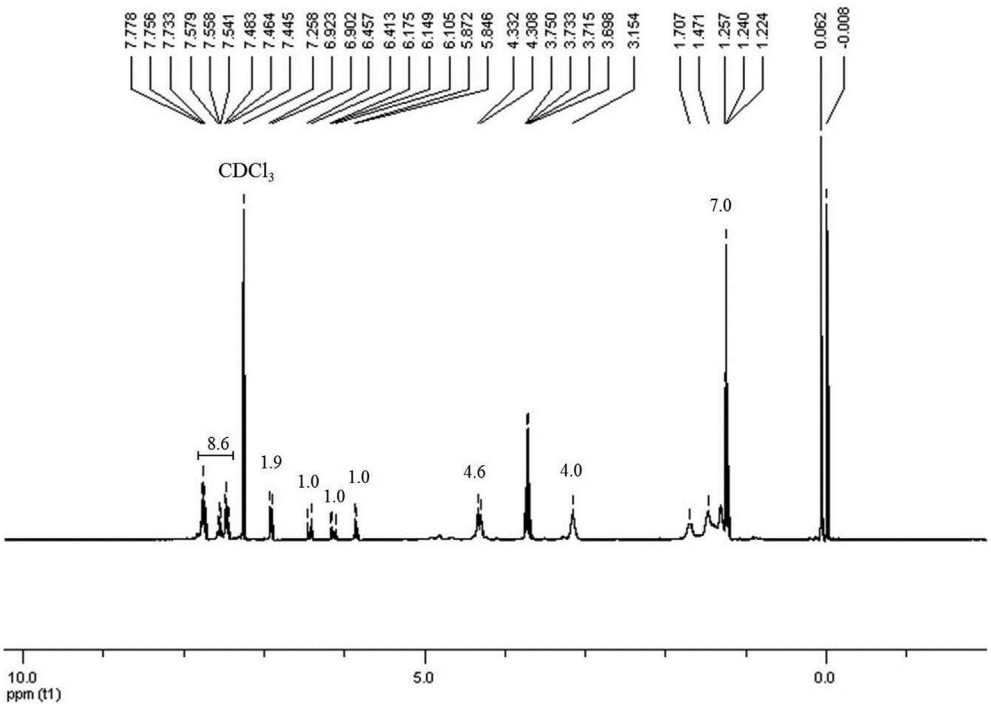

Fig. 3. ^{1}H NMR spectrum of BPA.

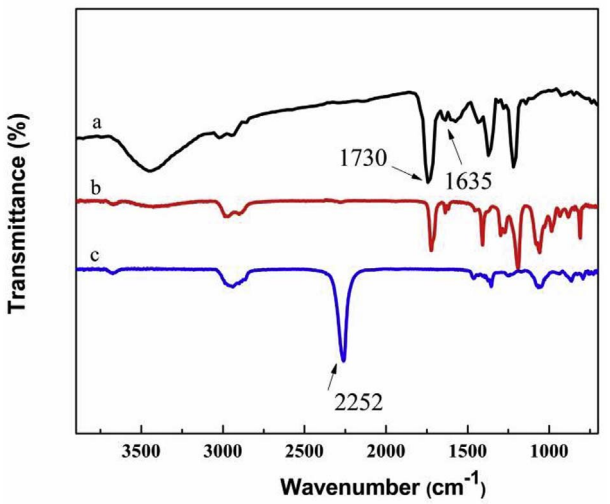

Fig. 4. FTIR spectra of a) BPA; b) 2-HEA; c) HDI.

product was obtained after dried in rotary evaporator at 50 °C for 1 h. The characterization data of MASR was provided in supporting information.

2.2.2. Preparation of BPA

In a three-necked 500 mL flask equipped with a magnetic stirrer, a reflux condenser, a thermometer and a N_2 gas inlet, a solution of HDI (2.35 g, 14 mmol) in DMF was added. The temperature was then raised to 50 °C and a solution of 2-HEA (1.63 g, 14 mmol) in DMF containing dibutyltin dilaurate (0.5 wt%) was added dropwise into the flask. The reaction mixture was maintained at 50 °C for 8 h till the concentration of NCO reached the theoretical value (the percentage of residual NCO groups was determined by typical dibutylamine chemical titration). Then, the solution of 4-hydroxybenzophenone (2.78 g, 14 mmol) in DMF was added dropwise over a period of 1 h and reacted with the residual NCO groups at 65 °C for 15 h with adding extra dibutyltin dilaurate (1.0 wt%). The precipitated product was isolated by suction filtration and dried in vacuum oven.

2.2.3. Preparation rGO-TiO_2 composites

Graphene oxide (GO) was prepared by a modification of Hummers' method [22]. RGO-TiO_2 composites were synthesized hydrothermally. Briefly, the volume ratio of ethanol/water was 75:5 in this reaction system. The weight ratios of raw material $Ti(OC_4H_9)_4$/GO were 400:1, 200:1, 100:1 and 50:1, which were denoted as rGO-TiO_2-1, rGO-TiO_2-2, rGO-TiO_2-3, and rGO-TiO_2-4, respectively. The reactants was maintained and stirred at 80 °C for 12 h and then poured into a Teflon-lined autoclave for hydrothermal reaction at 200 °C for 5 h. Finally, rGO-TiO_2 composites were collected after washed repeatedly with ethanol and deionized water and dried. Then different rGO-TiO_2 percentage of the resins by weight (1%, 2%, 5%, 10%) was added into silicone resin to evaluate their influence on UV-curing reactivity and thermal stability.

2.3. Characterizations

Fourier transform infrared (FTIR) spectra in the range of 4000–400 cm^{-1} were obtained by a Nicolet FTIR 5700 spectrometer (USA). The molecular weight of the obtained methacrylic-silicone resins was characterized by gel permeation chromatography (GPC, Water 515, Waters, USA), using THF as an eluent and polystyrene as the standard. ^{1}H NMR and ^{29}Si NMR spectra were provided from a Bruker WM500 (Germany). UV spectra were analyzed utilizing a UV–vis spectrophotometer (Model Lambda 900, USA). The X-ray diffraction (XRD) data were acquired from a Shimazdu X-ray diffractometer. The X-ray photoelectron spectroscopy (XPS) was analyzed with a VG electron spectrometer having a 0.3–0.5 eV resolution from a monochromated aluminum anode X-ray source using Kα radiation with 1486.6 eV (ESCALAB Mk II, UK). The Raman spectra of the samples were performed using a laser confocal Raman spectrometer (Renishaw inVia, England). The thermal stability of the UV-cured samples were studied on a NETZSCH thermoanalyzer (STA449C, made in Germany) under a nitrogen atmosphere with the heating ramp of 20 °C/min from 30 to 900 °C.

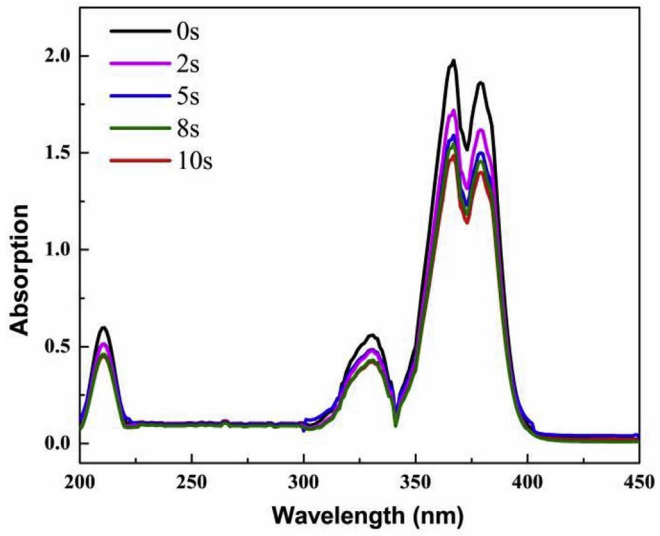

Fig. 5. UV absorption spectrum of BPA (1 wt%) in MASR solution with different UV radiation time.

3. Results and discussion

3.1. Synthesis and structural characterization of BPA

In order to enhance UV-curing reactivity and the conversion of the C=C double bonds of MASR, polymerizable photoinitiator containing acryloxy was prepared (see Fig. 2). To avoid the side reaction, the intermediate (HDHA) was firstly synthesized by HDI and 2-HEA with catalyst dibutyltin dilaurate, then benzophenone was incorporated into HDHA in order to obtain the BPA. The molecular structure of the target product was confirmed by ^{1}H NMR and FTIR (Fig. 3 and Fig. 4).

The structure of BPA was characterized by ^{1}H NMR and FTIR. In ^{1}H NMR spectrum (Fig. 3), the signals at 1.224–1.257 ppm, 3.154 ppm and 4.308–4.332 ppm are assigned to the methylene protons, indicating the existence of methylene group derived from the HDI and 2-HEA. The chemical shift at 6.902–6.923 ppm is attributed to amino protons and the aromatic protons are detected at the range of 7.445–7.778 ppm. The protons of –HC=CH$_2$ appear at 5.846–6.457 ppm. The characteristic ^{1}H NMR data of the synthesized compound was given in Table S3.

The expected structure of BPA was further evidenced by FTIR as depicted in Fig. 4. For BPA, the characteristic peak at 1730 cm^{-1} assigned to the stretching vibration of C=O can be observed and the absorption band located at 1635 cm^{-1} is ascribed to C=C. The feature at 3444 cm^{-1} refers to the stretching vibration of secondary amine group –NH–. The peaks at 2800–2900 cm^{-1} indicate that –CH$_2$ are existed in the target products. Besides, the characteristic stretching vibration of –NCO group completely disappears in FTIR spectrum, indicating the successful synthesis of BPA.

UV absorption spectra are utilized to analyze the absorption property of BPA (see Fig. 5). The maximum of absorption of BP is around 250 nm, which can be attributed to the main benzenoid π-π* type transition [23]. However, BPA exhibits a markedly red-shifted maximal absorption, which may be ascribed to the strong electron-donation effect via the influence of substitutional group [21]. It can be found that the higher maximal absorption is beyond 300 nm, which is much higher than those polymerizable photoinitiators [24], and is similar to the thioxanthone photoinitiator [25]. It is well known that the maximal absorption of photoinitiators is very important in terms of their photochemical activity. Thus, the red-shifted maximum makes BPA attractive as a photoinitiator, suitable for UV-curing near the visible spectrum. In addition, the absorption intensity decreases as irradiation time increases. At the end of the irradiation, the higher maximal absorbance reduces from 1.979 to 1.485, suggesting that the photoinitiators are consumed as the photolysis proceeds.

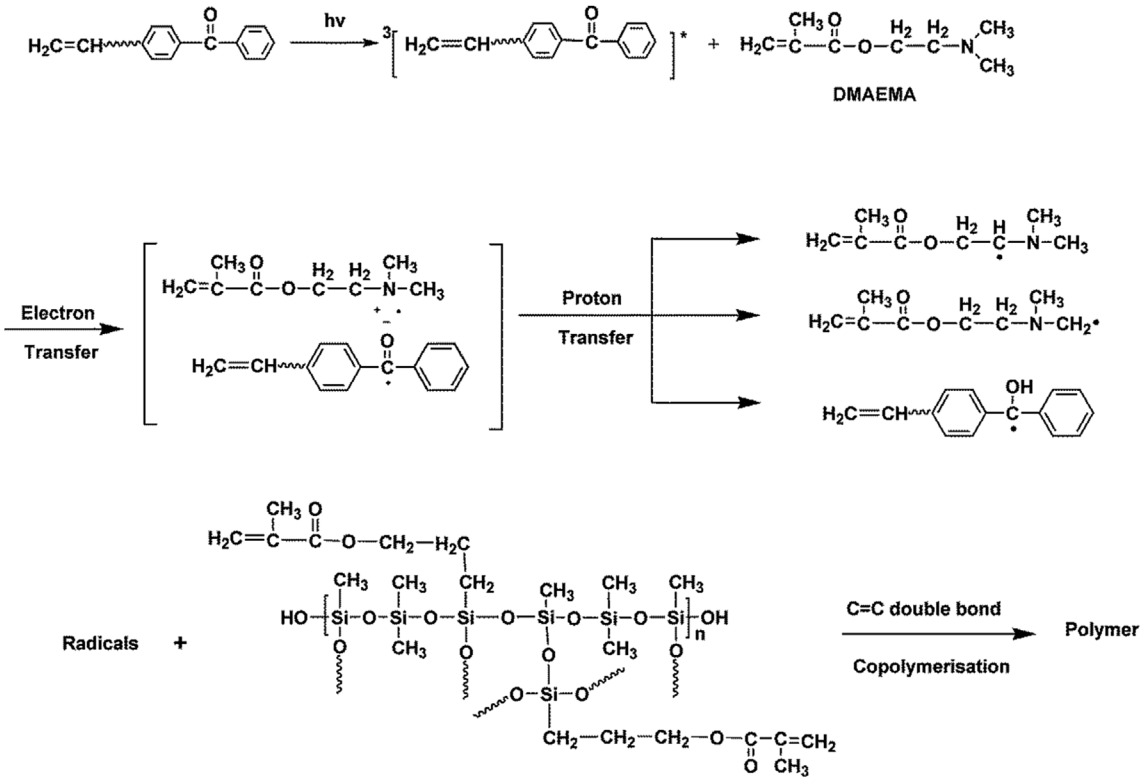

Fig. 6. Photoreaction mechanism of MASR initiated by BPA.

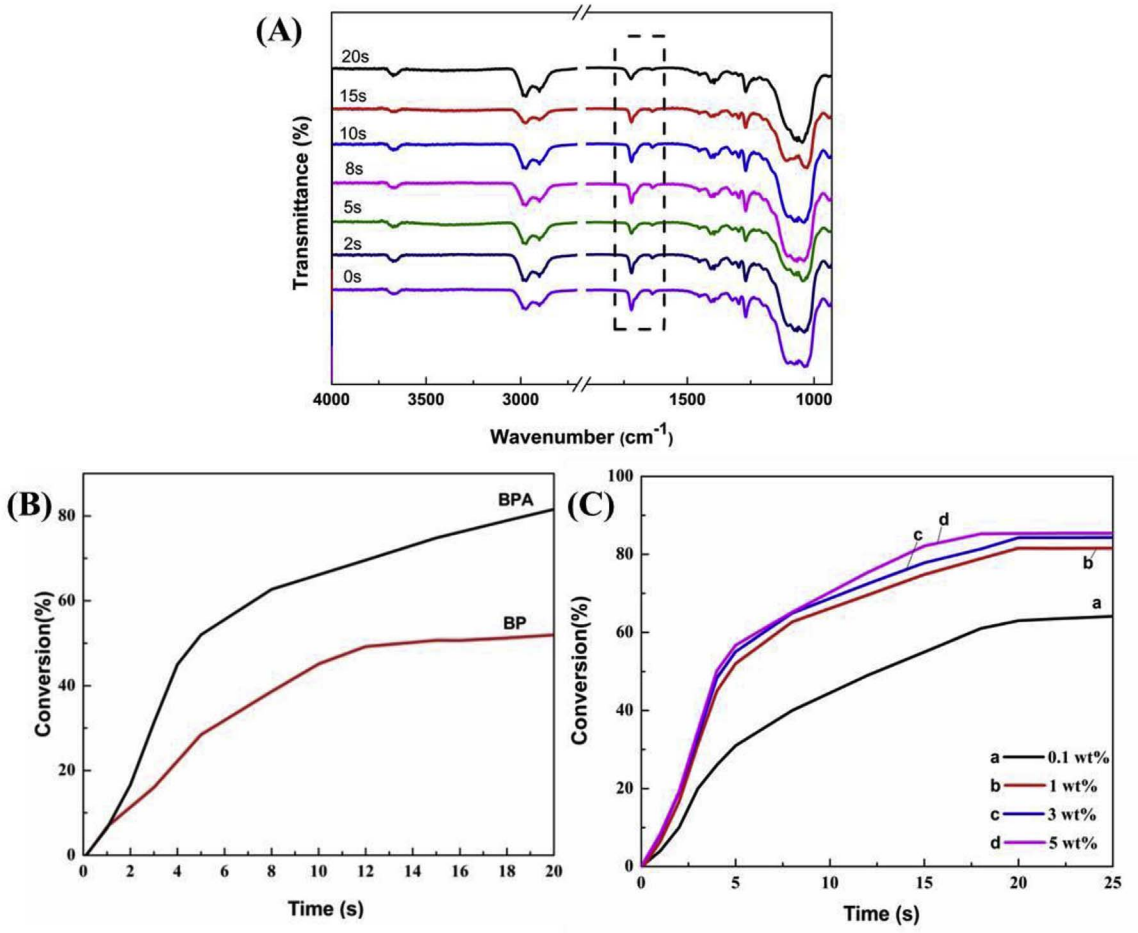

Fig. 7. (A) FTIR spectra of polymerization of MASR initiated by BPA with different UV radiation time. (B) Conversion versus time for photopolymerization of MASR initiated by BPA and BP. (C) Conversion versus time for photopolymerization of MASR using different concentrations of BPA.

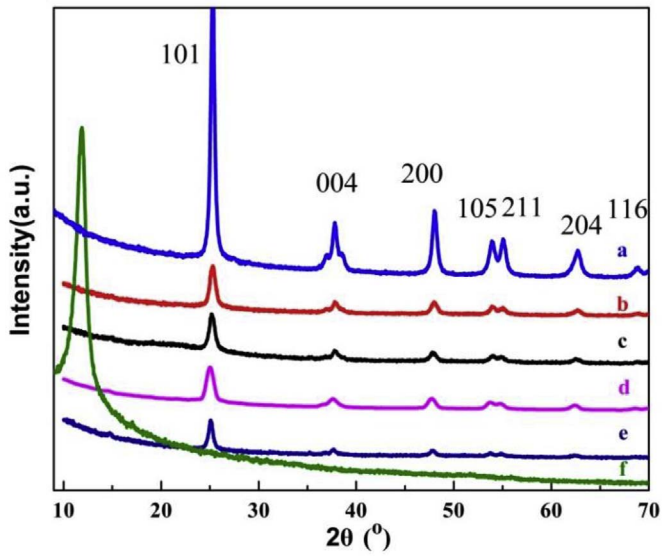

Fig. 8. XRD pattern of a TiO_2; b rGO-TiO_2-1; c rGO-TiO_2-2; d rGO-TiO_2-3; e rGO-TiO_2-4 and f GO.

3.2. UV-curing of MASR based on BPA

Photosensitive methacrylic was incorporated into silicone resin molecular chain. The designed molecular structure of MASR was manifested in Fig. S1. The photolysis of benzophenone could produce a radical which comes from the carbonyl compound and another radical derives from coinitiators. However, steric hindrance and electronic delocalization make these ketyl-type radicals unreactive agents [25]. The photopolymerization of the MASR containing carbon-carbon double bonds is initiated exclusively by active amine radicals [26], as shown in Fig. 6. BPA containing acryloxy could not only generate radicals from the photolysis reaction, also could be consumed via copolymerizing with MASR during polymerization, which significantly reduces the migration of the active species.

UV curing behaviors of MASR was studied via FTIR spectroscopy as shown in Fig. 7(A). The relative conversion percentage of unsaturated carbon-carbon double bonds in MASR was determined from the integration of the absorption band of the reactive functionality (C=C peak at around 1638 cm^{-1}) after normalization by a constant signal in the spectra (C=O peak at around 1720 cm^{-1}) [27]. Thus, the conversion of the carbon-carbon double bonds or the extent of reaction could be determined by integrating the peak area according to the following eqn,

$$W = \left\{1 - \frac{(A_{1638}/A_{1720})_t}{(A_{1638}/A_{1720})_0}\right\} \times 100\%$$

Where A_0 is the area of absorption peak before UV exposure and A_t is the area of absorption peak after UV exposure.

The double bonds conversion of MASR with different UV exposure time initiated by BP and BPA (1 wt%) was shown in Fig. 7(B). The final conversion degree of BP/DMAEMA photoinitiator system only reaches 52% with 20 s UV radiations. Compared with BP, the BPA is much more efficient, as the final conversion reaches 81% after UV radiation 20 s.

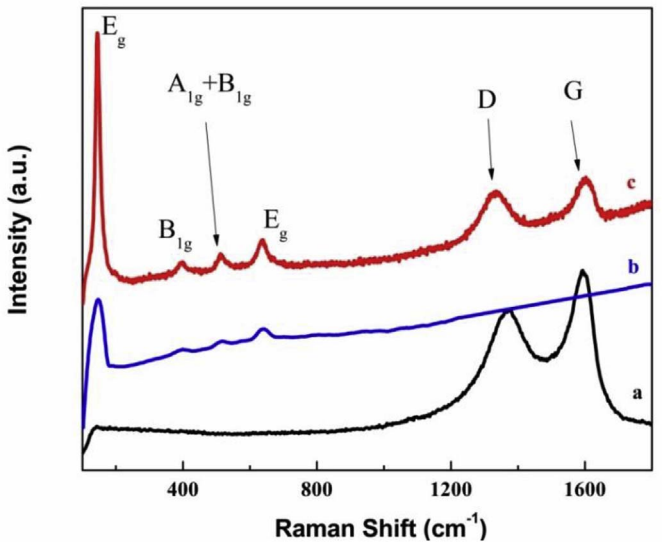

Fig. 9. Raman spectra of a GO; b TiO_2; c rGO-TiO_2.

The high photoefficiency of BPA may be ascribed to the higher electron/proton transfer rate between BPA and DMAEMA and the red-shifted maximal UV absorption of BPA [28]. The polymerizable photoredox system significantly may reduce the migration of the active species, leading to a high efficiency. Fig. 7(C) further illustrates that the effect of the photoinitiator concentration on the photopolymerization of MASR. With the addition of BPA concentration, the carbon-carbon double bonds conversion increases. After 20 s UV exposure, the double bonds conversion reaches 63% when the concentration of BPA is 0.1 wt %. And the carbon-carbon double bonds conversion increases to 81% with 1 wt% BPA. However, when the concentration of BPA increases from 1 wt% to 5 wt%, the double bonds conversion of silicone resins has little difference. So in this system the optimal concentration of BPA was 1 wt% which was used in the following.

3.3. UV-curing of MASR based on BPA and rGO-TiO_2

RGO-TiO_2 composites were added into MASR to evaluate their influence on UV-curing reactivity and thermal stability. Fig. 8 shows the XRD patterns of the TiO_2, GO and rGO-TiO_2 composites. It can be found that rGO-TiO_2 and pure TiO_2 having a series of diffraction signals at 25.4, 37.7, 48.0, 53.9, 55.1, 62.6 and 68.9° refer to (101), (004), (200), (105), (211), (204), and (116) planes, respectively and is indexed to anatase phase of TiO_2 [29]. Additionally, the intensities of the diffraction peaks present a slight decline with the increasing of GO. The average crystal size of TiO_2 and rGO-TiO_2 are determined through the Scherrer formula to be about 5 nm and 10 nm, respectively [30]. These results prove that TiO_2 doping with GO has little impact on TiO_2 phase structure. Besides, the diffraction peak of GO decreases with the introduction of TiO_2 in the composites, suggesting the conversion of GO to rGO.

As an indicator of existence of TiO_2 and GO in composite material,

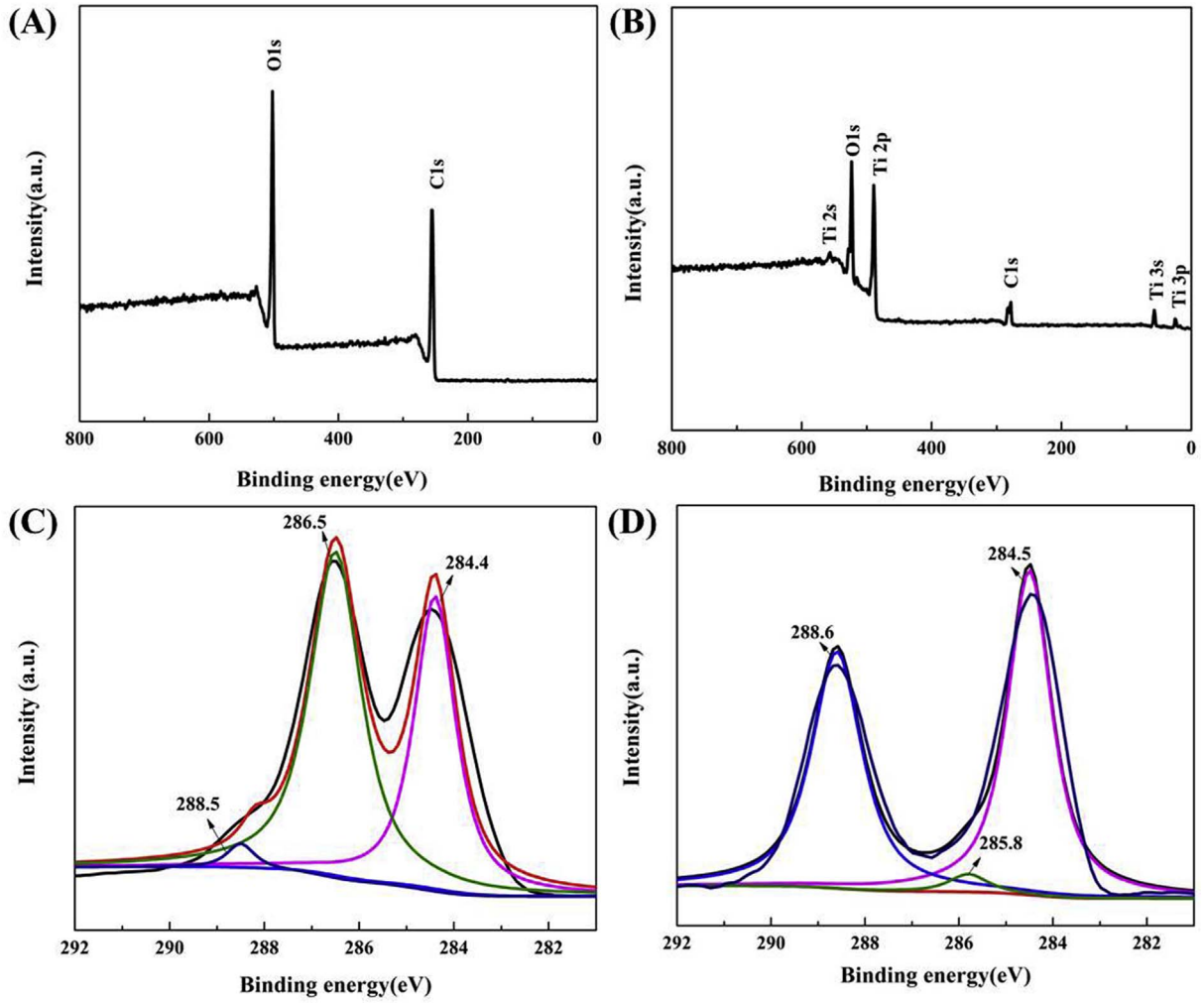

Fig. 10. XPS of (A) wide scan of GO; (B) wide scan of rGO-TiO_2; (C) deconvolution C1s spectra of GO; (D) deconvolution C1s spectra of rGO-TiO_2.

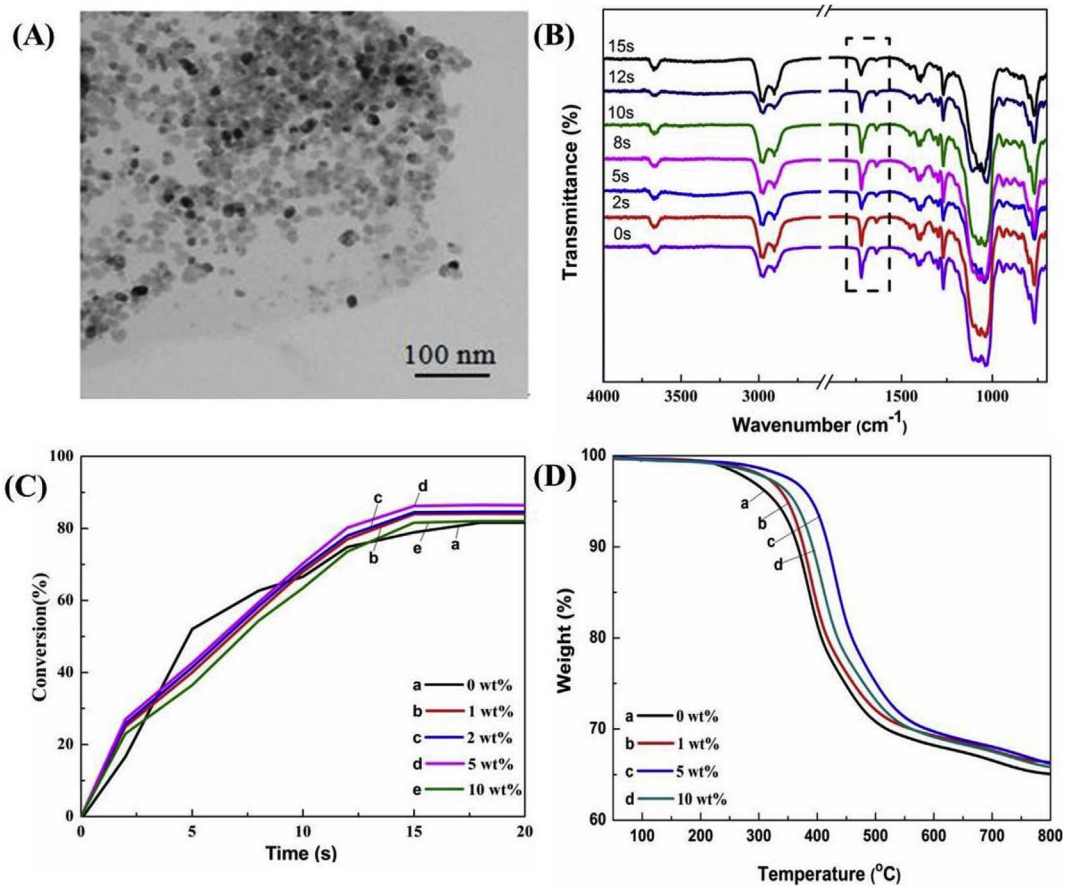

Fig. 11. (A) The microstructure of rGO-TiO_2 (B) FTIR spectra of polymerization of MASR initiated by BPA and rGO-TiO_2 with different UV radiation time. (C) Conversion versus time for photopolymerization of MASR using different concentrations of rGO-TiO_2. (D) TGA curves of MASR with different concentrations of rGO-TiO_2 under nitrogen atmosphere.

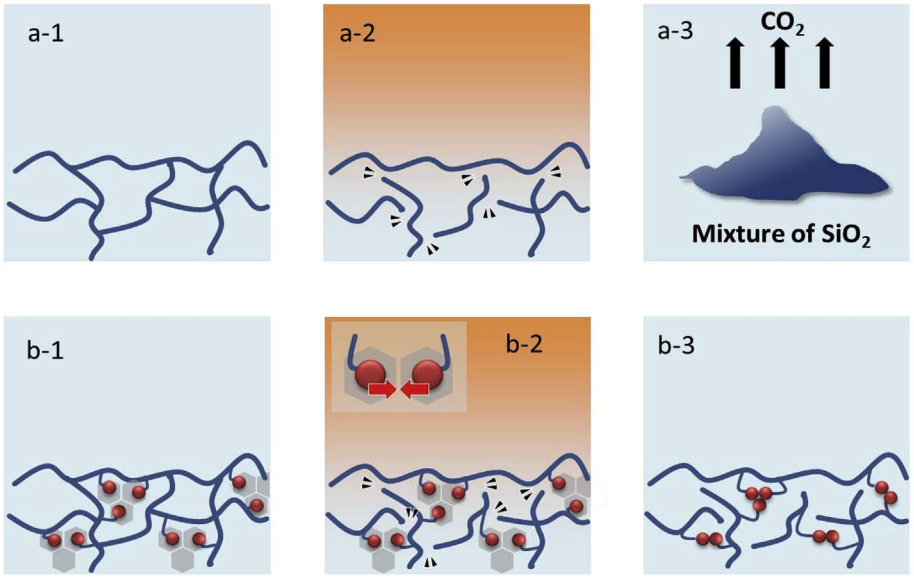

Fig. 12. Degradation sketch of the UV-cured MASR.

the Raman spectra were recorded (see Fig. 9). The four bands located at around 145 (E_g), 396 (B_{1g}), 518 (A_{1g} + B_{1g}), and 639 cm^{-1} (E_g) are characteristic for pure anatase TiO_2. The E_g bands are assigned to symmetric stretching vibrations of O–Ti–O, while the A_{1g} and B_{1g} bands refer to the symmetric and asymmetric bending vibration modes of O–Ti–O bonds [31]. Besides, there are two typical characteristic peaks at around 1370 and 1595 cm^{-1}, corresponding to the D and G bands of graphite, respectively [32]. Additionally, the D/G intensity ratio shows a significate increase for rGO-TiO_2 nanocomposite compared with that of GO, suggesting that the defects are increased after the reduction of GO [33].

To further confirm the structure of rGO-TiO_2, XPS analysis was taken and the spectrum was prepared in Fig. 10. The wide-scan XPS spectrum of rGO-TiO_2 shows that the rGO-TiO_2 contained C, Ti and O. For GO, the main peak observed at 284.4 eV is assigned to the presence of C–C, C = C, and C–H bonds of sp^2 carbon in GO [34]. The binding

energy peaks of 286.5 eV and 288.5 eV are corresponding to C–O and O–C = O, respectively [35]. For rGO-TiO_2, the decrease in C–O peak intensity is an indicator that the oxygen-containing functional groups have been partially reduced.

The microstructure of the rGO-TiO_2 nanocomposite was observed by TEM analysis as shown in Fig. 11(A). The capability of rGO-TiO_2 to promote the curing reaction can be explained by considering that, under UV light, photo-generated electron-hole pairs at the TiO_2 surface. Graphene can play the role of electron receptor and transporter for TiO_2, and the lifetime of electron-hole pair can be enhanced significantly. Therefore, the synergistic effects from graphene and TiO_2 could further enhance the carbon-carbon double bonds conversion in UV-curing silicone resins system initiated by BPA [16].

The behavior of rGO-TiO_2 in MASR and in promoting conversion of its methacrylic moieties was studied by FTIR spectroscopy. The carbon-carbon double bonds conversion in the formulation was followed by monitoring the decrease in the absorbance at 1638 cm^{-1} which was same with Fig. 7(A). As seen in Fig. 11(C), the presence of more rGO-TiO_2 particles involves an increase in the carbon-carbon double bonds conversion of MASR. In fact, the maximum conversion value has been recorded 86% at a 5 wt% rGO-TiO_2 loading after 15 s UV radiations, with an increase of 6.2% compared to BPA triggered system (20 s). However, more rGO-TiO_2 (10 wt%) results in a decreased conversion. The conversion curves confirm that a higher photopolymerization conversion is achieved in shorter reaction time for the formulation containing the rGO-TiO_2 with respect to the above sample (Fig. 7(C)), demonstrating that the embedded rGO-TiO_2 significantly increase UV-curing reactivity of the neat organic formulation.

Thermal stability of the UV-cured MASR and its subsequent nanocomposites were evaluated through the determination of the degradation temperature at 5% weight loss ($T_{5\%}$) and the residual weight at 800 °C (Y_c). Fig. 11(D) shows the TGA curves of all the samples. The $T_{5\%}$ and Y_c of the unfilled resin are 327.1 °C and 65.1%, respectively. These parameters are all increased with the increase of the rGO-TiO_2 amount, reaching their highest values with 5% rGO-TiO_2. In fact, $T_{5\%}$ increases to 389.6 °C and Y_c at 800 °C reaches a value of 66.2%. The enhancements seen in $T_{5\%}$ are related to the shielding effect of the rGO-TiO_2 that act as a barrier reducing the motion and insulating the materials from the heat source [36,37]. However, the $T_{5\%}$ and Y_c of the MASR decrease when the rGO-TiO_2 increases to 10%, which may be arising from the aggregation of nanoparticles and consequently leads to poorly disperse in the polymer matrix.

The degradation sketch of the MASR was shown in Fig. 12. Fig. 12(a-1) shows the molecular chair of the MASR. At high temperature, the Si–OH end groups have reacted and the Si–CH_3 groups in the resin are oxidized, releasing CO_2 and H_2O while SiO_2 remained in the crucible (Fig. 12(a-2) and Fig. 12(a-3)) [38]. However, the existence of rGO-TiO_2 significantly affects the degradation of the polymer matrix. When temperature increased, nanostructure tends to incorporate into the silicone molecular chain and avoid the condensation of the Si–OH. Thus, rGO-TiO_2 nanostructure on the silicone molecular chain plays a critical role in preventing the degradation of polymer molecular chain.

4. Conclusion

In summary, we have reported an efficient technique to enhance the polymerization degree of photosensitive methacrylic-silicone resins via polymerizable photoinitiator and rGO-TiO_2. The results indicate that BPA containing acryloxy is an efficient photoinitiator, which could generate radicals from the photolysis reaction and be consumed via copolymerizing with the methacrylic-silicone resins. The UV-cured MASR possesses a high carbon-carbon double bonds conversion above 80% initiated by BPA after 20 s UV radiations. Furthermore, the synergistic effects from graphene and TiO_2 further enhance the carbon-carbon double bonds conversion to 86% in shorter reaction time (15 s). Besides, the rGO-TiO_2 improved the thermal stability of the UV-cured MASR. Based on these findings, it can be concluded that the designed photoinitiator and rGO-TiO_2 nanocomposites could be applied in the photopolymerizable silicone resin and UV-curing fields.

Acknowledgements

This work was financially supported by Grant No. 51673054 from the National Natural Science Foundation of China.

Appendix A. Supplementary data

Supplementary data related to this article can be found at http://dx.doi.org/10.1016/j.compositesb.2017.12.006.

References

[1] Ren Z, Yan S. Polysiloxanes for optoelectronic applications. Prog Mater Sci 2016;83:383–416.
[2] Jiang B, Zhang K, Zhang T, Xu Z, Huang Y. Investigation of reactivity and biocompatibility poly-p-phenylene benzobisoxazole fiber grafted hyperbranched polysiloxane. Compos Part B B 2017;121:1–8.
[3] Soucek MD, Dworak DP, Chakraborty R. A new class of silicone resins for coatings. J Coat Technol Res 2007;4(3):263–74.
[4] Goff J, Sulaiman S, Arkles B, Lewicki JP. Soft materials with recoverable shape factors from extreme distortion states. Adv Mater 2016;28(12):2393–8.
[5] Nguyen KDQ, Megone WV, Kong D, Gautrot JE. Ultrafast diffusion-controlled thiol-ene based crosslinking of silicone elastomers with tailored mechanical properties for biomedical applications. Polym Chem 2016;7(33):5281–93.
[6] Dong J, Yang C, Cheng Y, Wu T, Zhao X, Zhang Q. Facile method for fabricating low dielectric constant polyimide fibers with hyperbranched polysiloxane. J Mater Chem C 2017;5(11):2818–25.
[7] Ingrosso C, Esposito Corcione C, Striani R, Comparelli R, Striccoli M, Agostiano A, et al. UV-curable nanocomposite based on methacrylic-siloxane resin and surface-modified TiO_2 nanocrystals. ACS Appl Mater Interface 2015;7(28):15494–505.
[8] Mustata F, Tudorachi N, Bicu I. Thermosetting resins obtained via sequential photo and thermal crosslinking of epoxy resins. Curing kinetics, thermal properties and morphology. Compos Part B B 2013;55:470–8.
[9] Yang B, Parada CM, Storey RF. Synthesis, characterization, and photopolymerization of polyisobutylene phenol (Meth)acrylate macromers. Macromolecules 2016;49(17):6173–85.
[10] Chen C-H, Wang J-J, Yen F-S. Application of a UV curable hard coating containing κ-aluminum oxide particles on poly (vinyl chloride) plastic tiles. Compos Part B B 2012;43(2):569–72.
[11] Liu R, Zhang X, Zhu J, Liu X, Wang Z, Yan J. UV-curable coatings from multiarmed cardanol-based acrylate oligomers. ACS Sustain Chem Eng 2015;3(7):1313–20.
[12] Behboodi-Sadabad F, Zhang H, Trouillet V, Welle A, Plumeré N, Levkin PA. UV-triggered polymerization, deposition, and patterning of plant phenolic compounds. Adv Funct Mater 2017;27(22). 1700127-n/a.
[13] Al Mousawi A, Dumur F, Garra P, Toufaily J, Hamieh T, Graff B, et al. Carbazole scaffold based photoinitiator/photoredox catalysts: toward new high performance photoinitiating systems and application in LED projector 3D printing resins. Macromolecules 2017;50(7):2747–58.
[14] Lalevée J, Blanchard N, Chany AC, El-Roz M, Souane R, Graff B, et al. Silyl radical chemistry and conventional photoinitiators: a route for the design of efficient systems. Macromolecules 2009;42(16):6031–7.
[15] Jiang B, Zhang T, Zhao L, Xu Z, Huang Y. Effect of Polymerizable Photoinitiators on the UV-polymerization behaviors of photosensitive polysiloxane. J Polym Sci, Part A: Polym Chem 2017;55(10):1696–705.
[16] Ingrosso C, Bianco GV, Pifferi V, Guffanti P, Petronella F, Comparelli R, et al. Enhanced photoactivity and conductivity in transparent TiO_2 nanocrystals/graphene hybrid anodes. J Mater Chem A 2017;5(19):9307–15.
[17] Parveen N, Mahato N, Ansari MO, Cho MH. Enhanced electrochemical behavior and hydrophobicity of crystalline polyaniline@graphene nanocomposite synthesized at elevated temperature. Compos Part B B 2016;87:281–90.
[18] Kwon YJ, Kim Y, Jeon H, Cho S, Lee W, Lee JU. Graphene/carbon nanotube hybrid as a multi-functional interfacial reinforcement for carbon fiber-reinforced composites. Compos Part B B 2017;122:23–30.
[19] Wang J, Chen Y, Liu G, Cao Y. Synthesis, characterization and photocatalytic activity of inexpensive and non-toxic Fe_2O_3-Fe_3O_4 nano-composites supported by montmorillonite and modified by graphene. Compos Part B B 2017;114:211–22.
[20] Zhang Y, Zhang N, Tang ZR, Xu YJ. Improving the photocatalytic performance of graphene-TiO_2 nanocomposites via a combined strategy of decreasing defects of graphene and increasing interfacial contact. Phys Chem Chem Phys 2012;14(25):9167–75.
[21] Wang H, Wei J, Jiang X, Yin J. Novel chemical-bonded polymerizable sulfur-containing photoinitiators comprising the structure of planar N-phenylmaleimide and benzophenone for photopolymerization. Polymer 2006;47(14):4967–75.
[22] Marcano DC, Kosynkin DV, Berlin JM, Sinitskii A, Sun Z, Slesarev A, et al. Improved synthesis of graphene oxide. ACS Nano 2010;4(8):4806–14.
[23] Liska R. Photoinitiators with functional groups. V. New water-soluble photoinitiators containing carbohydrate residues and copolymerizable derivatives

thereof. J Polym Sci, Part A: Polym Chem 2002;40(10):1504–18.
[24] Wang H, Wei J, Jiang X, Yin J. Effect of N-phenylmaleimide on a novel chemically bonded polymerizable photoinitiator comprising the structure of planar N-phenylmaleimide and benzophenone for photopolymerization. Polym Int 2007;56(2):200–7.
[25] Aydin M, Arsu N, Yagci Y. One-component bimolecular photoinitiating systems, 2. Macromol Rapid Commun 2003;24(12):718–23.
[26] Wei J, Jiang XS, Wang HY. Effect of the structure of photosensitive groups contained in novel PU-type polymeric benzophenone photoinitiators on photopolymerization. Macromol Chem Phys 2007;208(21):2303–11.
[27] Vitale A, Quaglio M, Chiodoni A, Bejtka K, Cocuzza M, Pirri CF, et al. Oxygen-inhibition lithography for the fabrication of multipolymeric structures. Adv Mater 2015;27(31):4560–5.
[28] Wei J, Wang H, Yin J. Novel polymeric, thio-containing photoinitiator comprising in-chain benzophenone and an amine coinitiator for photopolymerization. J Polym Sci, Part A: Polym Chem 2007;45(4):576–87.
[29] Yadav HM, Kim J-S. Solvothermal synthesis of anatase TiO_2-graphene oxide nanocomposites and their photocatalytic performance. J Alloys Compd 2016;688:123–9.
[30] Jiang B, Zhao L, Guo J, Yan X, Ding D, Zhu C, et al. Improved thermal stability of methylsilicone resins by compositing with N-doped graphene oxide/Co_3O_4 nanoparticles. J Nanopart Res 2016;18(6).
[31] Trapalis A, Todorova N, Giannakopoulou T, Boukos N, Speliotis T, Dimotikali D, et al. TiO_2/graphene composite photocatalysts for NOx removal: a comparison of surfactant-stabilized graphene and reduced graphene oxide. Appl Catal, B 2016;180:637–47.
[32] Kumari S, Shekhar A, Pathak DD. Graphene oxide-TiO_2 composite: an efficient heterogeneous catalyst for the green synthesis of pyrazoles and pyridines. New J Chem 2016;40(6):5053–60.
[33] Zhang X-Y, Li H-P, Cui X-L, Lin Y. Graphene/TiO_2 nanocomposites: synthesis, characterization and application in hydrogen evolution from water photocatalytic splitting. J Mater Chem 2010;20(14):2801.
[34] Prabhakarrao N, Chandra MR, Rao TS. Synthesis of Zr doped TiO_2/reduced Graphene Oxide (rGO) nanocomposite material for efficient photocatalytic degradation of Eosin Blue dye under visible light irradiation. J Alloys Compd 2017;694:596–606.
[35] Nawaz M, Miran W, Jang J, Lee DS. One-step hydrothermal synthesis of porous 3D reduced graphene oxide/TiO_2 aerogel for carbamazepine photodegradation in aqueous solution. Appl Catal, B 2017;203:85–95.
[36] Yang LW, Zhang XS, Liu HT, Zu M. Thermal resistant, mechanical and electrical properties of a novel ultrahigh-content randomly-oriented CNTs reinforced SiC matrix composite-sheet. Compos Part B B 2017;119:10–7.
[37] Qiu F, Hao Y, Li X, Wang B, Wang M. Functionalized graphene sheets filled isotactic polypropylene nanocomposites. Compos Part B B 2015;71:175–83.
[38] Jia P, Liu H, Liu Q, Cai X. Thermal degradation mechanism and flame retardancy of MQ silicone/epoxy resin composites. Polym Degrad Stab 2016;134:144–50.